MNRAS **469,** S339–S345 (2017)
Advance Access publication 2017 June 30
doi:10.1093/mnras/stx1621

Energy–angle dispersion of accelerated heavy ions at 67P/Churyumov–Gerasimenko: implication in the mass-loading mechanism

G. Nicolaou,[1★] E. Behar,[1,2] H. Nilsson,[1,2] M. Wieser,[1] M. Yamauchi,[1] Laura Berčič[1,2] and G. Stenberg Wieser[1]

[1]*Swedish Institute of Space Physics, SE-981 28 Kiruna, Sweden*
[2]*Department of Computer Science, Electrical and Space Engineering, Luleå University of Technology, SE-981 28 Kiruna, Sweden*

Accepted 2017 June 23. Received 2017 June 12; in original form 2017 March 30

ABSTRACT

The *Rosetta* spacecraft studied the comet 67P/Churyumov–Gerasimenko for nearly two years. The Ion Composition Analyzer instrument on board *Rosetta* observed the positive ion distributions in the environment of the comet during the mission. A portion of the comet's neutral coma is expected to get ionized, depending on the comet's activity and position relative to the Sun, and the newly created ions are picked up and accelerated by the solar wind electric field, while the solar wind flow is deflected in the opposite direction. This interaction, known as the mass-loading mechanism, was previously studied by comparing the bulk flow direction of both the solar wind protons and the accelerated cometary ions with respect to the direction of the magnetic and the convective solar wind electric field. In this study, we show that energy–angle dispersion is occasionally observed. We report two types of dispersion: one where the observed motion is consistent with ions gyrating in the local magnetic field and another where the energy–angle dispersion is opposite to that expected from gyration in the local magnetic field. Given that the cometary ion gyro-radius in the undisturbed solar wind magnetic and electric field is expected to be too large to be detected in this way, our observations indicate that the local electric field might be significantly smaller than that of the undisturbed solar wind. We also discuss how the energy–angle dispersion, which is not consistent with gyration, may occur due to spatially inhomogeneous densities and electric fields.

Key words: plasmas – comets: individual: 67P.

1 INTRODUCTION

The mechanism of mass-loading is common in the environment of comets (Szegö et al. 2000). A portion of a comet's neutral coma is ionized either by photoionization (by solar extreme ultraviolet radiation), or by charge-exchange with solar wind ions or by electron impact ionization (e.g. Wallis 1973; Mendis, Houpis & Marconi 1985; Cravens et al. 1988). The newly born cometary ions are then 'picked up' by the electric field of the solar wind and will start gyrating about the interplanetary magnetic field (IMF) (e.g. Neugebauer et al. 1987; Coates et al. 1989). The solar wind provides energy and momentum to the newly born ions. As a direct consequence of this interaction, the flow around the comet will have different characteristics from the undisturbed solar wind. The mass-loading is a function of the comet's outgassing rate, and it can vary significantly either due to the comet's activity or due to its distance from the Sun.

The mass-loading effect was previously observed at comet Halley (e.g. Balsiger et al. 1986; Johnstone et al. 1986; Korth et al. 1986; Mukai et al. 1986), Giaccobini–Zinner (Sanderson et al. 1986), Grigg–Skjellerup (Johnstone et al. 1993) and Borrelly (Young et al. 2004; Richter et al. 2011). In the environment of these comets, an interaction region was observed, where the solar wind was gradually slowing down and deflected away from the Sun–comet line as a result of the momentum exchange with the cometary pickup ions that had been added to the flow. Even though the mass-loading was observed by fly-by missions, prior to *Rosetta* there were no *in situ* long-term measurements of a changing comet environment.

Rosetta (Glassmeier et al. 2007) was launched in 2004 for its ∼10 yr long journey to the comet 67P/Churyumov–Gerasimenko (67P), and it was the first spacecraft to orbit around a comet, obtaining *in situ* measurements of its environment down to a few kilometres above its surface. The Rosetta Plasma Consortium (RPC) package (Carr et al. 2007) on board *Rosetta* consisted of five instruments, designed to measure the plasma properties in the vicinity of the comet. The Ion and Electron Sensor (IES; Burch et al. 2007)

★ E-mail: gnicolaou@irf.se

measured the ion and electron distributions in the energy-per-charge range of 1 eV/q to 22 keV/q. Goldstein et al. (2015) described the distributions of the low- and high-energy pickup ions observed by IES. They showed that those distributions are quite different from the ring-like distributions observed at very active comets (e.g. Neugebauer et al. 1987; Coates et al. 1989). In the case of 67P, the newly created ions are observed very close to the point where they were picked up by the solar wind; thus, their energy is still low and their trajectories are relatively linear.

Further analysis of the IES observations by Broiles et al. (2015) described in more detail the mass-loading process in the environment of a weakly outgassing comet, when 67P was ∼3 au far from the Sun. During the mass-loading process, the newly born cometary ions added to the system result in a lower bulk speed (sum of cometary ion speed and solar wind speed), which, in turn, slows down the IMF in the frozen-in description, giving rise to a Lorenz force in the solar wind proton frame. As a result, the solar wind protons are deflected up to 45° from the Sun–comet line, but they are not significantly slowed down.

Nilsson et al. (2015) reported on the first detection of water ions in the comet's environment by the Ion Composition Analyzer (ICA) instrument (Nilsson et al. 2007) on board *Rosetta*. The instrument detected the newly born ions at about 100 km from the comet, while the Sun–comet distance was ∼3.6 au and the comet was in a low-activity state. During the same period, the solar wind was barely disturbed, and the direction of the heavy ion flow was perpendicular to the solar wind flow direction, as would be expected for acceleration along the solar wind convective field. Later on, when the spacecraft approached the comet at ∼28 km and when the Sun–comet distance was ∼3.3 au, the water ion fluxes were enhanced and the solar wind was observed to be deflected by ∼25°.

Behar et al. (2016a) investigated the mass-loading in the comet's environment using ICA observations for a case when the comet was ∼2.88 au far from the Sun. For the specific case, the mass-loading was stronger than it was for the cases studied by Nilsson et al. (2015) since the comet was closer to the Sun. The authors derived the bulk flow directions of the deflected solar wind protons and the accelerated cometary ions. The bulk flow vectors were then compared to the local magnetic field direction, and it was shown that, to first order, the dynamics are driven by the local solar wind electric field $\boldsymbol{E} = -\boldsymbol{u}_{sw} \times \boldsymbol{B}$, where $\boldsymbol{u}_{sw}$ is the solar wind velocity and $\boldsymbol{B}$ is the magnetic field vector. The flow and field directions were expressed using the clock and the cone angle of the normalized vectors in the body-Centred Solar EQuatorial (CSEQ) frame. It was shown that the bulk flow direction of the accelerated cometary ions lies in the same plane as the deflected solar wind flow and the solar wind electric field. However, the fact that the direction of the accelerated heavy ions is not aligned with the $-\boldsymbol{u}_{sw} \times \boldsymbol{B}$ field indicates that the simplistic calculation of the local convective field from solar wind proton speed and magnetic field is at least not a precise approximation, especially when the mass-loading is significant. There is also the possibility that another field(s) is contributing to the interaction, for example, a polarization electric field, as discussed briefly also by Nilsson et al. (2015) and extensively by Behar et al. (2016a).

Behar et al. (2016b) compared ICA observations with hybrid simulations for six different cases at heliocentric distances ranging from ∼2 to 3.6 au. The simulations agree with the observations and show deflections of the solar wind, which are anticorrelated with the heliocentric distance. The simulation predicts a very small deceleration of the solar wind protons, according to the observations, but the observed deflection angle is larger than the deflection seen in the model.

There are many time intervals when ICA observes a clear energy–angle dispersion of the accelerated cometary water ions. The correlation between the energy and flow direction seems to differ from time to time, which is at first sight surprising, given the fact that the expected trajectories of the ions should be relatively straight due to their large gyro-radius. This aspect has not been studied previously in data from *Rosetta*. At larger, more active comets, ring or shell distributions were frequently observed; these give rise to energy–angle dispersion (Coates et al. 1989). In this study, we present two cases where the energy–angle dispersion is clearly observed by ICA but differs for each case. We characterize the dispersion in a comet-centred frame, and we discuss two simplified scenarios that could explain the observations. This paper is organized as follows. In Section 2, we briefly describe the ICA instrument and its detection principle. In Section 3, we describe our methodology, and in Section 4, we present two selected cases of energy–angle dispersion. We discuss the two cases in Section 5, and we finally report our main conclusions in Section 6.

2 INSTRUMENT

The ICA instrument (Nilsson et al. 2007) is a part of the RPC package, and it measures the distributions of plasma ions (positively charged) in the energy-per-charge range of ∼10 eV/q to ∼40 keV/q. The field of view (FOV) of the instrument (Fig. 1) covers 360° in azimuth (top-hat analyser plane) and ∼90° in elevation (with respect to the symmetry axis that is vertical to the top-hat plane). The azimuthal FOV is covered by 16 sectors covering 22.5 each. The elevation direction is achieved by the use of electrostatic deflections, and it is divided into 16 elevation steps with an approximate width of ∼5°. As particles enter the instrument's aperture, they fly towards the electrostatic analyser, which consists of two conductive hemispherical plates that sit on different voltages, resulting in a potential difference that guides the particles through the analyser. As the voltage difference between the two analyser plates changes, ions with different energy-per-charge are detected. Voltage sweeps (with up to 96 steps, depending on the used energy table during individual scans) give the full energy range. The energy resolution of the instrument is $\Delta E/E = 0.07$. Ions that pass the electrostatic analyser enter a region of a toroidal magnetic field, achieved by permanent magnets. In that region, ions with the same energy-per-charge but with different mass-per-charge will follow different trajectories under the influence of the Lorenz force. The ions of lower mass-per-charge are being deflected farther away from the vertical symmetry axis and hit the multichannel plate detector at a larger radial distance. The mass detection is accomplished by 32 equally separated bins (mass rings or anodes). For a more detailed description of the instrument, see Nilsson et al. (2007).

3 METHODOLOGY

We identify dispersion events observed by the ICA instrument by examining the energy–mass, energy–elevation angle and energy–azimuth angle matrices [similar to what is shown in Fig. 2(a)–(c)] that cover one day of observations each. The energy–mass matrix shows the amount of counts (time integrated) detected in each mass bin (radial distance from vertical symmetry axis) as a function of energy. The mass bins where specific species are detected for a given energy are determined from pre-flight calibration. The energy–azimuth/elevation angle matrices [Fig. 2(b) and (c)] show

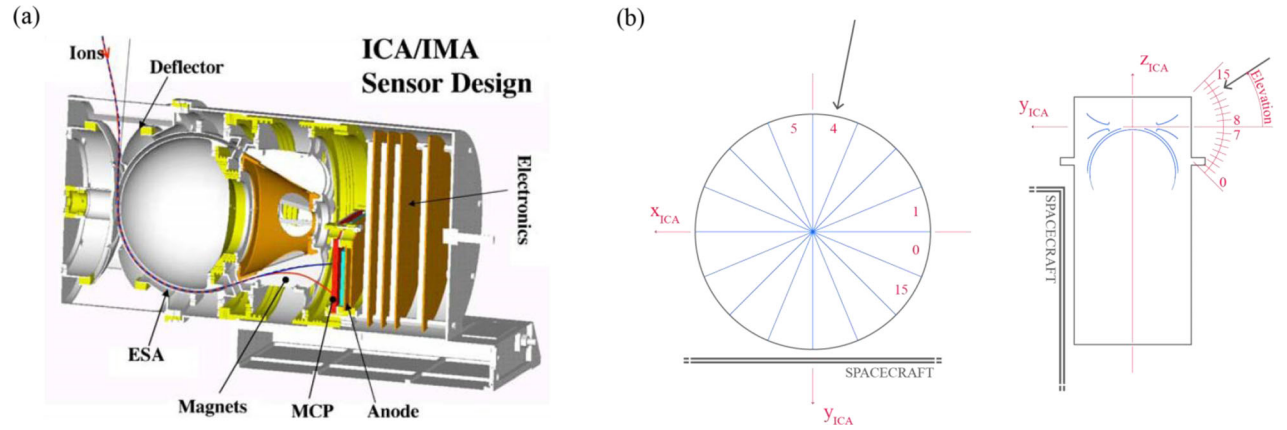

Figure 1. (a) Cross-section of the ICA instrument showing its main components. The schematic shows trajectories of different m/q ions (blue and red lines) for a given voltage setting of the electrostatic analyser plates. The ions with different m/q follow different trajectories in the region where the magnets are installed, and they are finally detected by a position sensitive detector. (b) The azimuth FOV (16 sectors) and the elevation FOV definition in the instrument's frame (adapted from Nilsson et al. 2007).

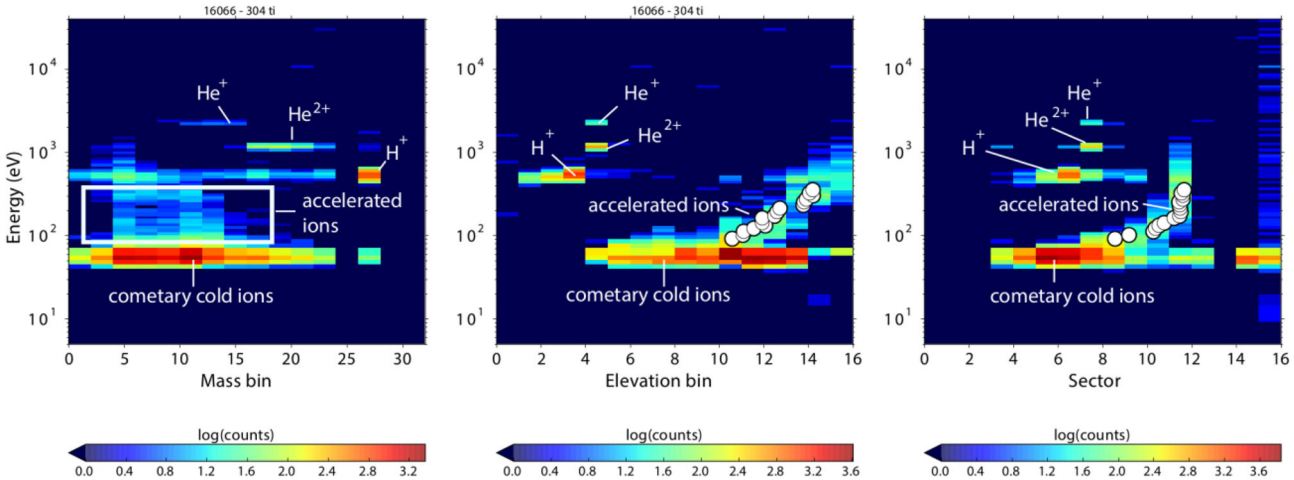

Figure 2. Example of an energy–angle dispersion event. Plot (a) shows the mass–energy matrix of a full single elevation–energy scan at 2016 March 9 11:20:31 UT. The signature of the accelerated ions is marked within the white box. Plot (b) shows the elevation–energy matrix for the same scan. The white dots indicate the average elevation for each energy bin for the accelerated ion population, as it is calculated with our method. Plot (c) shows the corresponding azimuth–energy matrix for the same scan.

the counts (time integrated) as a function of elevation/azimuth flow direction (instrument's frame) and energy. The dispersion is identified as a characteristic pattern (increase or decrease) of the flow angles as a function of energy. Thus, we identify the dispersion event in the azimuth and elevation matrices first, and the mass matrix is checked to confirm that the dispersed ions are actually cometary, heavy ions. When an energy–angle dispersion event is found in the daily matrices, we manually determine the energy range where it is clearly observed, and then we investigate, one by one, the 192-s energy–elevation scans obtained during that day. During the cases presented here, the instrument sweeps 96 energy steps in 12 s; thus, a full energy–elevation scan is completed in $16 \times 12 = 192$ s. For each energy step within the selected energy range, we calculate the average azimuth and elevation direction of the dispersed ions by taking the mean value weighted by counts (see Fig. 2). Consistently with the study of Behar et al. (2016a), we characterize the flow direction using the cone angle: the angle between the selected flow and the comet–Sun line, in the range $[0^\circ, 180^\circ]$. This cone angle is computed for each energy step, within each scan. We need to mention that the observed dispersion is identified in energies above ~100 eV, and therefore the effects of the spacecraft potential (maximum $|V| \sim 20$ V) on the trajectories of the ions in such energies can be considered minor.

To complete the set of representations of the data, the differential energy flux of the accelerated cometary ions (with energy above 100 eV) is given in the velocity space (lower panels of Figs 3 and 4). These distributions are integrated over 1 h (20 scans) of measurements. Before the integration, the distribution for each scan is rotated around the comet–Sun line, from the instrument reference frame to the following frame: The x-axis is given by the sunward direction, and the calculated bulk velocity is placed in the (x, z) plane. The y-axis completes this right-handed particle-aligned reference frame. We represent the averaged projection of these energy flux distributions in the three Cartesian planes. (The relevance of this frame is discussed in the next section.)

4 RESULTS

After surveying the ICA observations covering a period from 2014 August to 2016 September, we identified cases where the

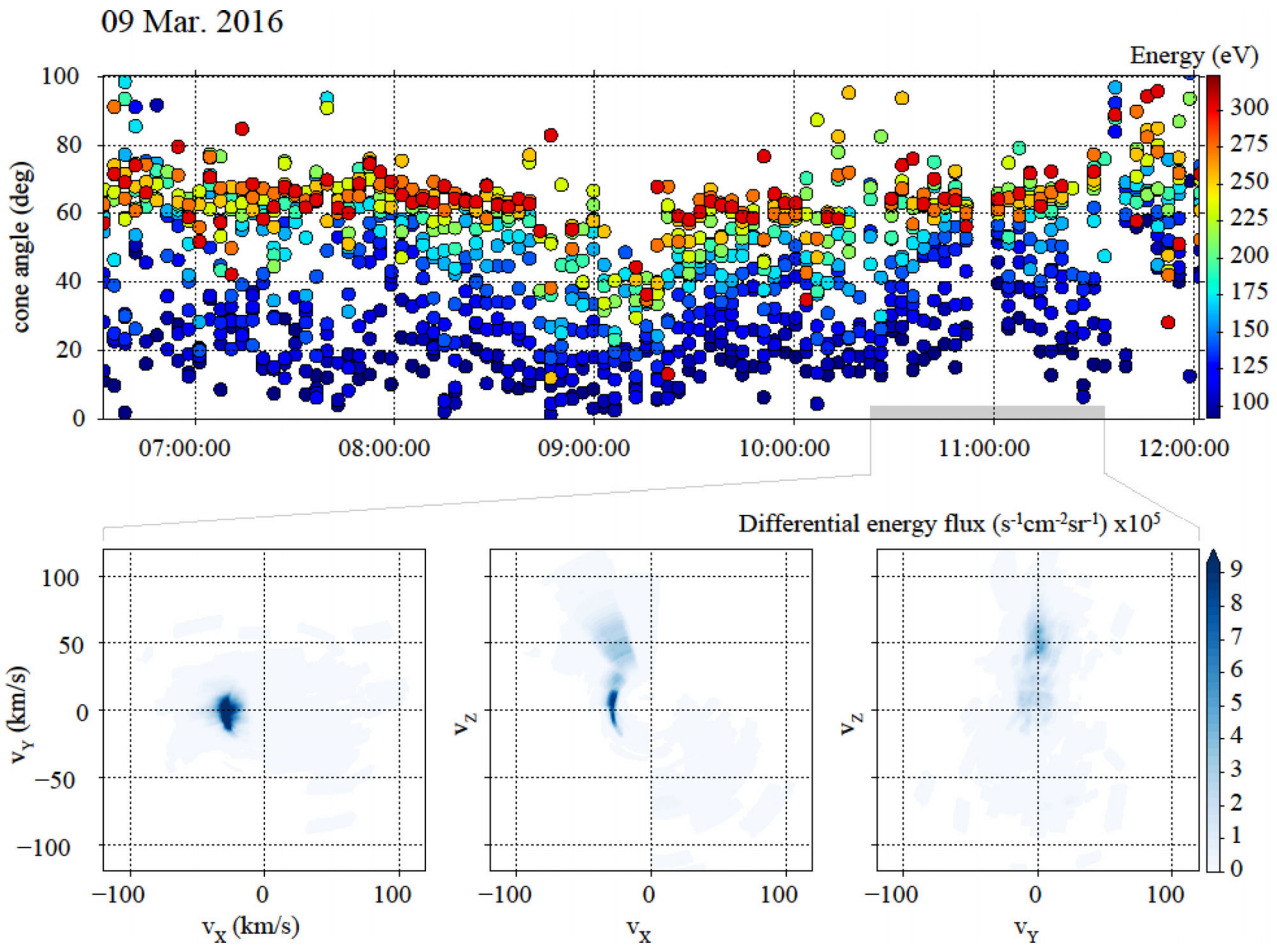

Figure 3. Observation of a positive-dispersion event on 2016 March 9. The upper panel shows the cone angle of the accelerated ions flow versus time. Each energy step (instrument's energy scan steps) is shown in different colour (blue to red = low to high energy). The three panels in the bottom show the differential energy flux for an interval of ∼1 h (20 elevation–energy scans) of the event (indicated by the grey line in the upper panel).

accelerated cometary ions show clear energy–angle dispersion. In general, dispersion events are observed during different phases of the mission, but in this study we present two typical cases that exhibit two different types of energy–angle dispersion. Potential future studies would aim for a complete statistical and quantitative analysis of all the detected cases.

We show two cases: one where the cone angle of the flow increases with energy (positive dispersion) and the other where the cone angle decreases with energy (negative dispersion). Table 1 summarizes the observation environment for each event. Among others, we provide the heliocentric distance and the distance between the spacecraft and the nucleus during the observation of each event and the estimated H_2O^+ production rate from the model of Hansen et al. (2016). In addition, we provide the position of the spacecraft in the CSEQ frame, where X_{sceq} is along the comet–Sun line (pointing towards the sun), Z_{cseq} is towards the Sun's north pole and Y_{cseq} completes the right-handed orthogonal system.

Fig. 3, upper panel, shows the cone angle of the accelerated heavy ions as a function of time for an interval of ∼6 h during 2016 March 9, where a positive-dispersion event is observed. The specific event was recorded when the comet was ∼2.5 au far from the Sun and the spacecraft was ∼17 km far from the nucleus. The corresponding plot for a negative dispersion is shown in Fig. 4, upper panel, for an interval of ∼6 h during 2015 December 8, observed when the comet was ∼1.8 au far from the Sun and the spacecraft was ∼110 km far from the nucleus. Each time stamp of the plots represents one full energy–elevation scan and the energy is colour coded; for each time stamp (each scan), we show the flow cone angle of the dispersed ions as determined for each energy step with a dot of different colour. The colour bar on the side of each plot shows the energies corresponding to each colour.

At the lower panels of Figs 3 and 4, we show the differential energy flux of the heavy ions in a particle flow aligned frame, as described in the previous section. When rotated along the comet–Sun line and then integrated, we see that the differential energy flux distributions have little spread along the V_Y axis, whereas the previously identified dispersion is clearly seen extending in the (V_X, V_Z) plane. This means that the particle trajectories are mostly contained in a single plane for each measurement. According to Behar et al. (2016a), this plane would rotate together with the upstream magnetic field, which is expected to be perpendicular to V_Z. We note that on 2015 December 8 (during the negative dispersion case), the spacecraft was still in the solar wind cavity reported by Behar et al. (2017). The solar wind reappeared at the spacecraft location just three days later.

5 DISCUSSION

In this study, we investigate the cometary ion energy–angle dispersion by examining the cone angle of the ion flow as a function

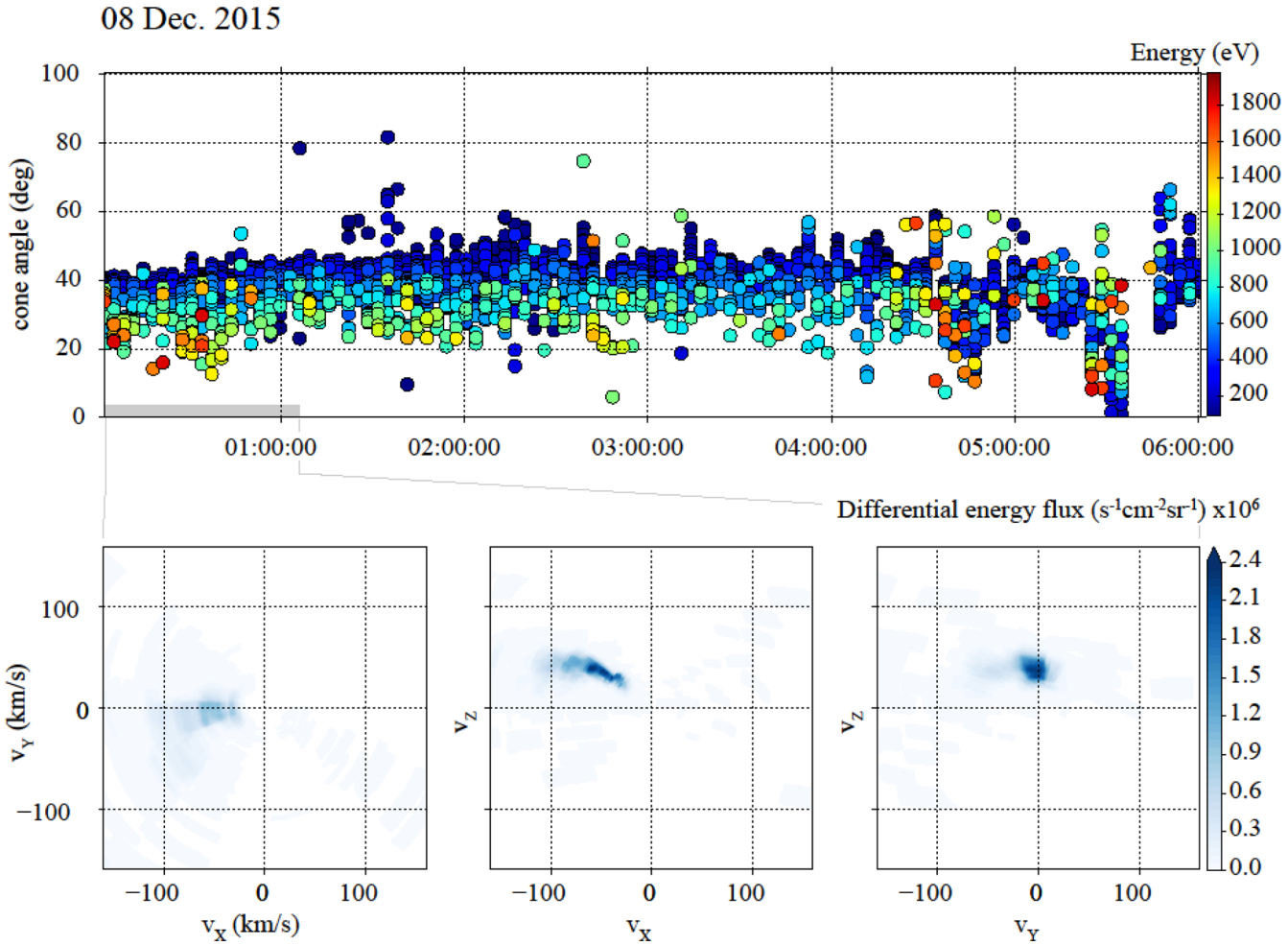

Figure 4. Observation of a negative-dispersion event represented with the same format as Fig. 3. The dispersion is seen clearly in the V_X–V_Z plane as a partial ring centred in the negative V_X direction.

Table 1. Basic parameters of the two dispersion cases we report in our study.

Parameter/ case type	Date	Distance from the Sun (au)	Distance from comet (km)	Solar wind energy (eV)	*B* field (nT)	H_2O production rates H_2(#/s)	spacecraft position in CSEQ frame X_{cseq} (km)	Y_{cseq} (km)	Z_{cseq} (km)
Positive dispersion	2016 March 9	2.5	17	400–600	5–45	$\sim 2 \times 10^{26}$	0	0	–17
Negative dispersion	2015 December 8	1.8	110	Not observed	5–45	$\sim 2 \times 10^{27}$	0	80	–70

of energy. Our analysis showed the characteristic correlation of cone angle and energy for the two different types of dispersion we detect in the data. The characteristic range of the cone angles and energies is estimated for each event. More specifically, during the positive-dispersion event on 2016 March 9, the cone angles are largely dispersed (over ∼60°). On 2015 December 8, during a negative-dispersion event, the typical cone angle difference ranged from ∼20° to ∼40°. We also note that the distribution in the negative dispersion case extends over a larger speed range (above 100 km s^{-1}) than in the positive case. We remind the reader that the FOV of the ICA instrument is limited (Section 2). If the dispersed flow is extended in elevation angles beyond the instrument's coverage, then the actual ranges will be higher than those we estimated from the observations.

The acceleration of the newly born heavy ions in the vicinity of the comet has been studied before, in terms of the ion bulk flow direction with respect to the local convective electric field, which was approximated by $\boldsymbol{E} = -\boldsymbol{u}_{sw} \times \boldsymbol{B}$. It was concluded that the convective electric field calculated just from the solar wind proton velocity and the local magnetic field is not a good approximation of the total local electric field at a medium comet activity, and/or another field contributes to the interaction (Behar et al. 2016a). This study implements another feature of the dynamics, that of the energy–angle dispersion.

The two dispersion cases we investigate in this paper are observed under different conditions (Table 1); thus, it is not unreasonable to expect different mechanisms driving the dynamics in each case. Most importantly, the expected water ion production rate

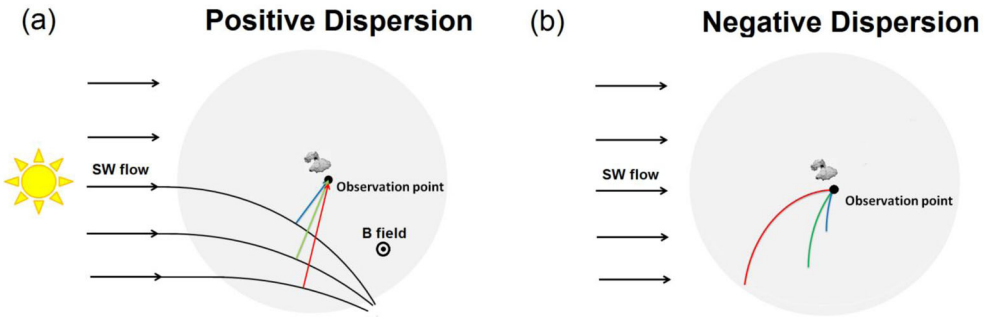

Figure 5. Two simple scenarios that can result in the observed dispersion cases of the accelerated ions. The red, green and blue lines indicate trajectories of heavy ions with different energy (acceleration), while the grey-shaded area represents the coma (not to scale or actual shape) for both cases. (a) Positive dispersion: The solar wind flow is deflected during the mass-loading process, while heavy cometary ions are accelerated along the $\boldsymbol{E} = -\boldsymbol{u}_{sw} \times \boldsymbol{B}$ field. (b) Negative dispersion: gyro-motion of the heavy ions within the coma (see the text for more details).

during the observation of the negative event at ∼1.8 au is one order of magnitude higher than the production rate expected during the positive-dispersion event observed at ∼2.5 au. To explain the observations of ion energy–angle dispersion, we sketch two different extremely simple scenarios, one for each case. Both scenarios assume no-collisions. The fact that we observe the directional flow of the ions in energies above ∼100 eV indicates that the dynamics are not driven by the binary collisions with the neutrals and that the charge-exchange collisions are not frequent enough to neutralize the newly born ions before they are accelerated to the observed energies.

Note that we do not attempt to address in detail the physical mechanisms responsible for the observations, but we try to give a general idea of the mechanism leading to the dispersion.

Scenario 1: Ions picked up by $\boldsymbol{E} = -\boldsymbol{u}_{sw} \times \boldsymbol{B}$ at different locations within the coma.

In the first scenario, the newly born heavy ions are accelerated by the motional convective electric field of the solar wind, $\boldsymbol{E} = -\boldsymbol{u}_{sw} \times \boldsymbol{B}$. Note that this scenario, corresponding to the test-particle dynamics, addresses the low-activity case. The gyro-radius of water ions in the solar wind frame, under the test-particle approach, for the observed solar wind speed and magnetic field during the specific event, ranges from 1300 to 12 000 km. With a gyro-radius larger than the source region probed by the spacecraft, the accelerated heavy ions follow nearly straight paths perpendicular to both the magnetic field and the solar wind flow vector. The solar wind flow that passes through regions closer to the comet is more deflected from the Sun–comet line, since it follows a longer path within the coma and goes through denser regions with more intense mass-loading. The heavy ions are created in the entire coma, and their flow direction in this simple model will be different as the solar wind flow direction is different at different locations. Since the accelerated ions that reach the instrument originate from different locations, they will therefore also have different flow directions. Fig. 5(a) shows the situation that corresponds to the positive-dispersion case. The flow of ions created farther away from the observation point has a higher cone angle (red trajectory). The ion energy will also be larger since the ions were accelerated for a longer time along their path from their origin to the observation point. According to this simplified scenario and for the typical solar wind speed and *B*-field magnitude during the dispersion event on 2016 March 9, we estimate that cometary ions were picked up within a region extending over ∼300 km. This means that the solar wind deflection is quite large over such a distance, given the spread of the ion flow direction (cone angle range over 60°). Alternatively, a contribution from an antisunward electric field, as discussed by Nilsson et al. (2015) and Behar et al. (2016a), would affect more the slower particles closer to the comet, thus increasing the spread of the cone angle accounted for by the scenario just described. It should also be noted that as the accelerated particles pass through different regions, they will experience a different acceleration since the electric field is changing (direction and/or magnitude). However, the resulting energy and direction are the result of the integrated electric field the particle has passed through along its trajectory, and the general angle–energy relation indicated by our simplistic scenario should hold.

Scenario 2: Gyro-motion. Possible contribution from other electric field(s).

In this scenario, ions are gyrating in the local magnetic and electric fields [Fig. 5(b)]. This gyro-motion does not have a constant gyro-radius, since both fields are expected to be inhomogeneous in the vicinity of the nucleus. For instance, the magnetic field is seen piling up (Behar et al. 2016b; Goetz et al. 2017), and the absence of the solar wind during that day also illustrates the complexity of this electromagnetic environment. More specifically, during stronger mass-loading periods, both solar wind and cometary ions are gyrating and the test-particle approach that considers nearly non-deflected solar wind flows is not valid. In fact, the solar wind protons can be completely deflected away from a whole region around the comet, namely the solar wind cavity (Behar et al. 2017). As a consequence, the local electric field in this case cannot be approximated by the solar wind motional field, which, in any case, we cannot estimate since we do not observe the solar wind flow. But even if classical-ring or partial-ring distributions with constant radii are not expected, the ordering/morphology/topology of the distribution should be comparable: in terms of this study, a negative cone angle dispersion, for which particles originating farther away from the instrument will arrive at the observation point with smaller cone angles. This agrees well with the distribution in Fig. 4, which shows us what this complex gyro-motion might look like in such an environment.

We note that, as observed earlier, the distributions picture ions mostly flowing in a single plane, which is a strong support for such two-dimensional dynamics. In both scenarios, ions that are ionized farther away are observed with higher energy. The farther from the nucleus, the lower the densities, and, in fact, the energy flux decreases with increasing speed. Finally, as indicated earlier, the above scenarios present simplistic dynamics that may account for the observed dispersion. For a more detailed understanding of the solar wind and cometary ion interaction, a statistical study of the

dispersion cases accompanied with modelling is needed, which is outside the scope of this paper. Such a study could categorize the events according to their type (positive or negative), their strength (energy–angle slope), location of detection, solar wind flow (magnitude and direction), and *B*-field direction and strength.

6 CONCLUSIONS

We present two time intervals where ICA observed clear signatures of energy–angle dispersion of the heavy accelerated ions in the environment of the comet 67P. In one of the presented cases, the angle between the accelerated ion flow vector and the Sun–comet line is increasing as a function of the ion energy. The second case shows the opposite relation between flow angle and energy. We suggest that ions originating at different locations within the coma arrive at the observation point following paths with a different flow cone angle and an energy reflecting the path length. If we assume that the paths are nearly straight lines along the $-\boldsymbol{u}_{\rm sw} \times \boldsymbol{B}$ field, we explain a positive dispersion by taking into account the larger deflection of the solar wind flow closer to the comet.

In the case of negative dispersion, we discuss the possibility of curved trajectories, with a curvature that is quite larger than the one expected for simple gyro-motion about the solar wind magnetic field in the presence of the solar wind electric field. The negative-dispersion case we present here is observed inside the solar wind cavity, which suggests that there are possibly other mechanisms contributing to the pickup acceleration in the vicinity of the comet, rather than the convective electric field of solar wind. A polarization electric field cancelling part of the solar wind electric field would be consistent with such a smaller gyro-radius of the cometary ions.

REFERENCES

Balsiger H. K. et al., 1986, Nature, 321, 330
Behar E., Nilsson H., Stenberg Wieser G., Nemeth Z., Broiles T. W., Richter I., 2016a, Geophys. Res. Lett., 43, 1411
Behar E., Lindkvist J., Nilsson H., Holmström M., Stenberg-Wieser G., Ramstad R., Götz C., 2016b, A&A, 596, A42
Behar E., Nilson H., Alho M., Goetz C., Tsurutani B., 2017, MNRAS, this issue
Broiles T. W. et al., 2015, A&A, 583, A21
Burch J. L. et al., 2007, Space Sci. Rev., 128, 697
Carr C. et al., 2007, Space Sci. Rev., 128, 629
Coates A. J., Johnstone A. D., Wilken B., Jockers K., Glassmeier K.-H., 1989, J. Geophys. Res., 94, 9983
Cravens T. E., Kozyra J. U., Nagy A. F., Gombosi T. I., Kurtz M., 1988, Electron Impact Ionization in the Vicinity of Comets, in Comet Encounters. American Geophysical Union, Washington, DC
Glassmeier K-H., Boehnhardt H., Koschny D., Kührt E., Richter I., 2007, Space Sci. Rev., 128, 1
Goetz C., Volwerk M., Richter I., Glassmeier K.-H., 2017, MNRAS, preprint (arXiv:e-prints)
Goldstein R. et al., 2015, Geophys. Res. Lett., 42, 3093
Hansen K. C. et al., 2016, MNRAS, 462, 491
Johnstone A. et al., 1986, Nature, 321, 344
Johnstone A. D. et al., 1993, A&A, 273, L1
Korth A. et al., 1986, Nature, 321, 335
Mendis D. A., Houpis H. L. F., Marconi M. L., 1985, Fundam. Cosm. Phys., 10, 1
Mukai T., Miyake W., Terasawa T., Kitayama M., Hirao K., 1986, Nature, 299
Neugebauer M. et al., 1987, A&A, 187, 21
Nilsson H. et al., 2007, Space Sci. Rev., 128, 671
Nilsson H. et al., 2015, Science, 347
Richter I., Koenders C., Glassmeier K., Tsurutani B., Goldstein R., 2011, Planet. Space Sci., 59, 691
Sanderson T. R., Wenzel K.-P., Daly P., Cowley S. W. H., Hynds R. J., Smith E. J., Bame S. J., Zwickl R. D., 1986, Geophys. Res. Lett., 13, 411
Szegö K. et al., 2000, Space Sci. Rev., 94, 429
Wallis M. K., 1973, Planet. Space Sci., 21,1647
Young D. et al., 2004, Icarus, 167, 80

This paper has been typeset from a Microsoft Word file prepared by the author.